Supporting Information

Out-of-Plane Electromechanical Response of Monolayer Molybdenum Disulfide Measured by Piezoresponse Force Microscopy

Christopher J. Brennan[1,2], Rudresh Ghosh[1,2], Kalhan Koul [1,2], Sanjay K. Banerjee[1,2,3], Nanshu Lu[1,2,3,4,5], Edward T. Yu[1,2,3]**

[1]Microelectronics Research Center, University of Texas at Austin, Austin, TX 78758

[2]Deparment of Electrical and Computer Engineering, University of Texas at Austin, Austin, TX 78701 USA.

[3]Texas Materials Institute, University of Texas at Austin, Austin, TX 78712 USA

[4]Center for Mechanics of Solids, Structures and Materials, Department of Aerospace Engineering and Engineering Mechanics, University of Texas at Austin, Austin, TX 78712 USA

[5]Department of Biomedical Engineering, University of Texas at Austin, Austin, TX 78712 USA

* Corresponding authors:

Edward T. Yu, ety@ece.utexas.edu, 512-232-5167, MER 1.206M, 10100 Burnet Rd. Bldg 160, Austin, TX 78758

Nanshu Lu, nanshulu@utexas.edu, 512-471-4208, 210 E. 24th St, Austin, TX 78712

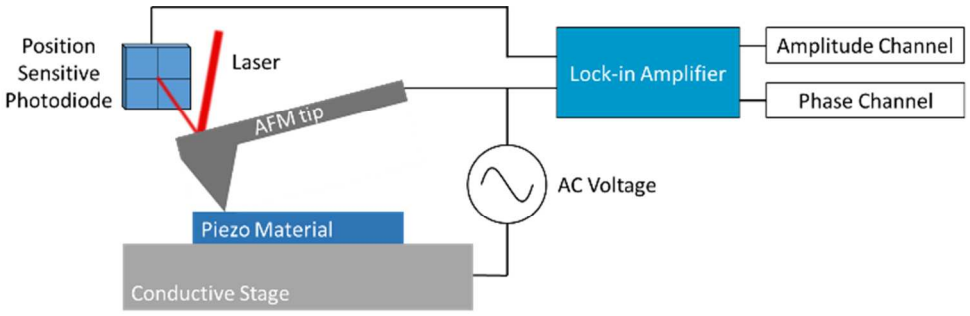

Figure S1. A schematic showing the PFM process and the tip sample geometry. An AC voltage is applied across the material to be measured. The AC voltage is also routed to a lock-in amplifier which uses its frequency as the reference frequency. The AC voltage causes a corresponding alternating expansion and contraction in the piezoelectric material which is measured as a laser deflection in a position sensitive photodiode (PSD). This signal is fed into the lock-in amplifier and the frequency component at the reference frequency is amplified. The lock-in amplifier outputs two different channels, the amplitude and phase of the amplified signal.

Supporting Note 1: *Equation for* d_{33}^{eff} *From Raw PFM Data*

The d_{33}^{eff} values given in this paper required processing from the raw data captured by the PFM. Two channels of data are captured in a PFM measurement: the piezoresponse amplitude and the piezoresponse phase (see Figure S1). The piezoresponse amplitude channel is captured as a voltage produced by laser movement on a position sensitive photodiode. The voltage is then converted into physical deflection by measuring the deflection sensitivity, s_d, of the AFM cantilever. This is done by measuring how much the laser is deflected in the PSD for a known vertical movement. Also during the PFM measurement, a hardware gain of 16x is used to enhance the signal. Based on these factors d_{33}^{eff} is then given by

$$d_{33}^{eff} = \frac{(PR\ AMP)\cdot s_d}{V_d \cdot GAIN}. \quad \text{(S1)}$$

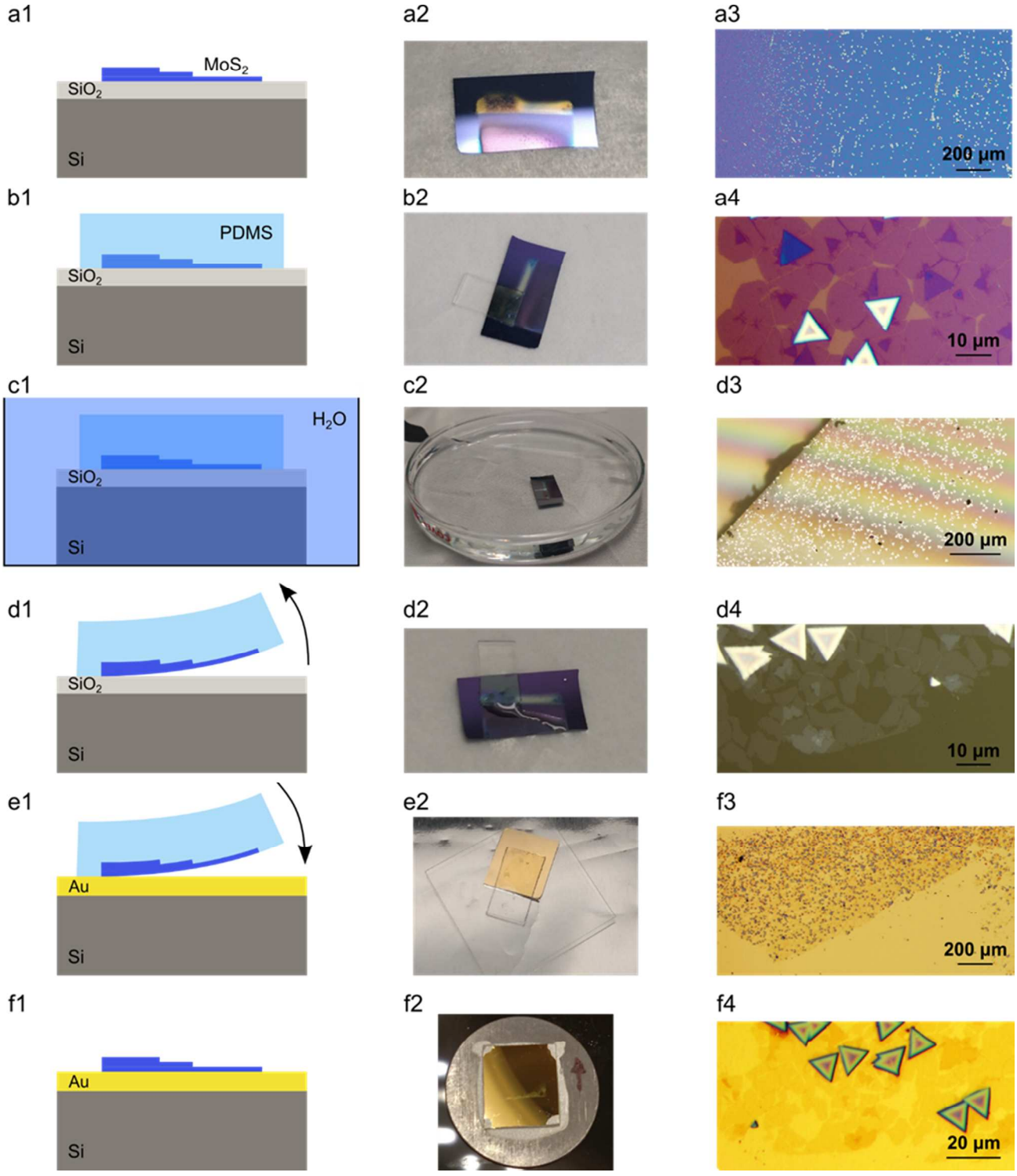

Figure S2. The transfer process of CVD grown MoS_2 is shown schematically in (**a1-f1)** and pictorially in (**a2-f2)**. The process flow is as follows: (**a1**) MoS_2 is grown on SiO_2 via CVD, (**b1**) a PDMS stamp is pressed on the MoS_2, (**c1**) the sample is submerged in water, (**d1**) the sample is removed from water,

dried, and the PDMS is peeled off with some MoS_2, (**e1**) the MoS_2 on PDMS is placed on the receiving substrate, gold shown here, and heated on a hot plate to 50 °C, (**f1**) finally the PDMS stamp is slowly peeled away, leaving the MoS_2 on the receiving substrate. Microscope images at two different magnifications show the MoS_2 on the growth substrate (**a3-4**), on the PDMS stamp (**d3-4**), and on the gold substrate (**f3-4**). Due to the PDMS being soft, strain from bending can cause cracking of the MoS_2 during the transfer process. This type of damage will not affect our PFM measurements.

Supporting Note 2: *MoS_2 Thickness Determination and Optical Characterization Difficulty*

AFM step height measurements on 2D materials have been shown to be somewhat unreliable and dependent on AFM measurement conditions[1,2]. This is exacerbated if the 2D material and its substrate have different mechanical properties[3–5]. Additionally, obtaining step-height measurements on substrates which have a roughness on the order of the film thickness is difficult. We have also seen slight variation between different AFM measurements of the same sample. Despite this, we believe that we have reasonably confirmed that we are measuring monolayer MoS_2 on both substrates.

Figure S3 shows MoS_2 on gold. The AFM height profile shown in Figure S3b reveals that the MoS_2 measured in Figure 3 of the main text is monolayer. The Raman data in Figure S3d further confirms the presence of monolayer MoS_2, with an $A_{1g} - E^1_{2g}$ ($A'_1 - E'$) peak separation of 19.7 cm^{-1}. The photoluminescence (PL) data (Figure S3e) also shows a significantly higher intensity on the monolayer region than on the multilayer region.

The thickness of MoS_2 on Al_2O_3 is more difficult to characterize. Figure S4a shows a tapping mode AFM image of the sample measured with PFM in Figure 5. The monolayer step shows a height value thicker than expected for a monolayer. Different literature reports have shown that 2D material step height measurements can be somewhat unreliable[1,2] and can be affected by differences in the mechanical properties of the 2D material and its substrate[3–5]. These issues are often solved by preforming Raman and PL measurements to confirm the presence of monolayer MoS_2. This is unfortunately not possible in our

sample because these two techniques give very weak signals when on such a thin layer of Al_2O_3 on silicon.

The sample geometry does not allow enough light to be absorbed by the MoS_2 to give measurable Raman and PL data, as is indicated by the poor optical contrast in the optical microscope image in Figure 1. Typically, thicker dielectric layers create internal reflections of light that allow for an increased optical contrast and absorption of light in the 2D materials[4]. MoS_2 directly placed on a silicon substrate does not absorb enough light (and emission is quenched) to give a measurable Raman and PL signal[6]. Also, a recent study has shown that for the thickness of Al_2O_3 used in this paper (~5.3 nm), MoS_2 is expected to have a very poor optical contrast[7]. With this understanding, it is expected that the Raman and PL signals of thin MoS_2 on 5.3 nm Al_2O_3 on silicon will be weak. Thicker regions of MoS_2 that are optically visible do give a measurable signal, as shown in Figure 2. Other studies showing Raman and PL of MoS_2 on sapphire and thin Al_2O_3 seem to mostly be on bulk sapphire[8] or sufficiently thick (~50 nm) Al_2O3_3 to offer optical contrast in microscope images[7].

To overcome this, we characterize the MoS_2 remaining on the SiO_2 growth substrate after the transfer process. Figure S5 shows that the MoS_2 on the growth SiO_2 also shows slightly inflated thickness values as measured by the AFM. However, Raman data (Figure S5e) confirms that this area of MoS_2 is monolayer. The thickness of monolayer MoS_2 measured on the growth substrate and after being transferred to the Al_2O_3 is comparable. Also, no thinner areas of MoS_2 on Al_2O_3 or SiO_2 are found across the samples. In the calculation done in this work, the thickness of monolayer MoS_2 is chosen to be 0.65 nm because this has been agreed upon in the literature as the thickness of pristine MoS_2. Any deviations from this value measured by AFM in this paper are attributed to errors in the AFM measurement.

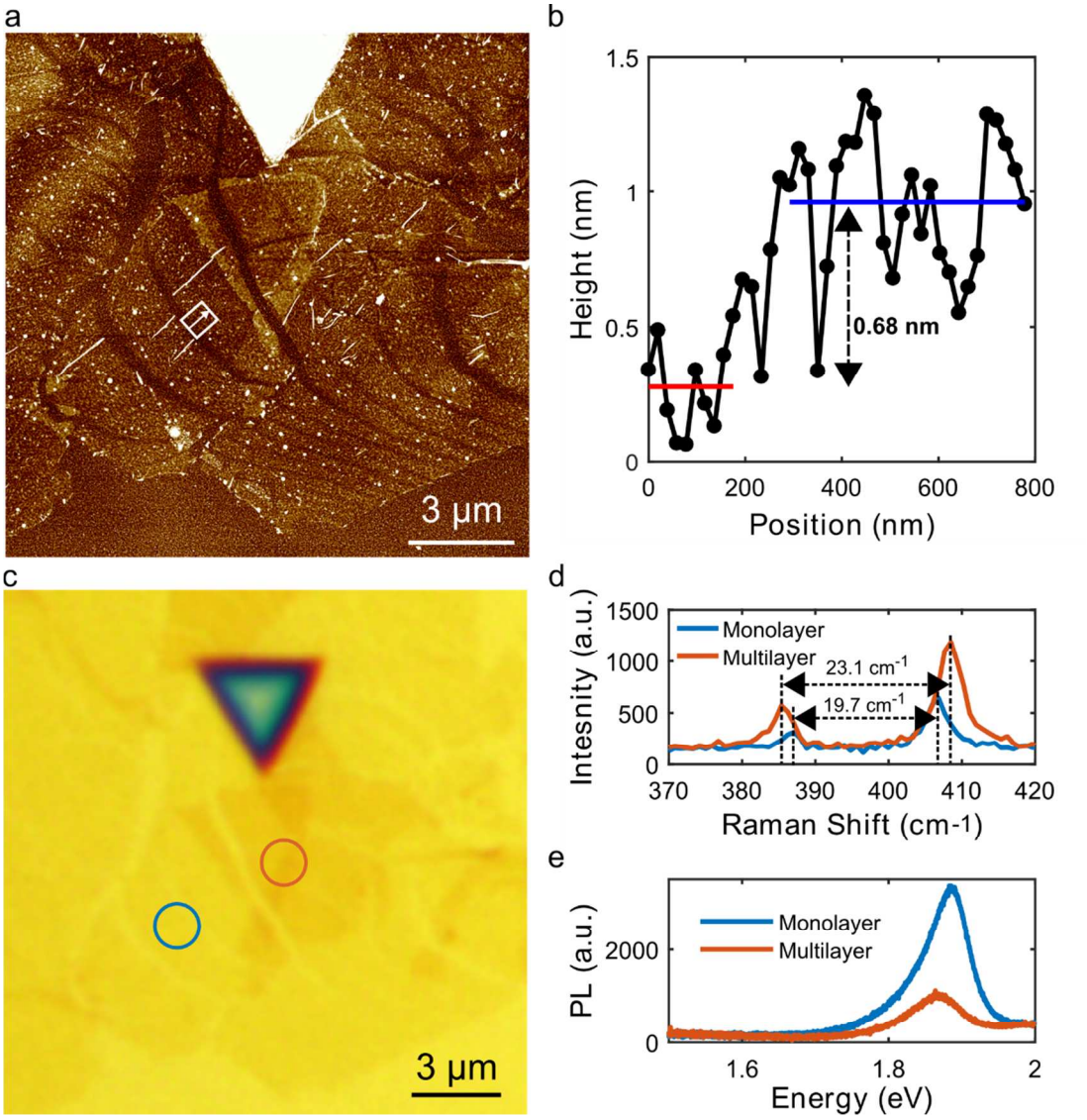

Figure S3. Tapping mode AFM image of MoS_2 on the gold substrate is shown in (**a**). A height profile is given for the white box in (**a**) where the width of the box indicates the area averaged to obtain (**b**). An optical microscope image is shown in (**c**). The blue and orange circles represent monolayer and multilayer MoS_2 measurement locations for Raman spectroscopy (**d**) and photoluminescence (**e**) measurements.

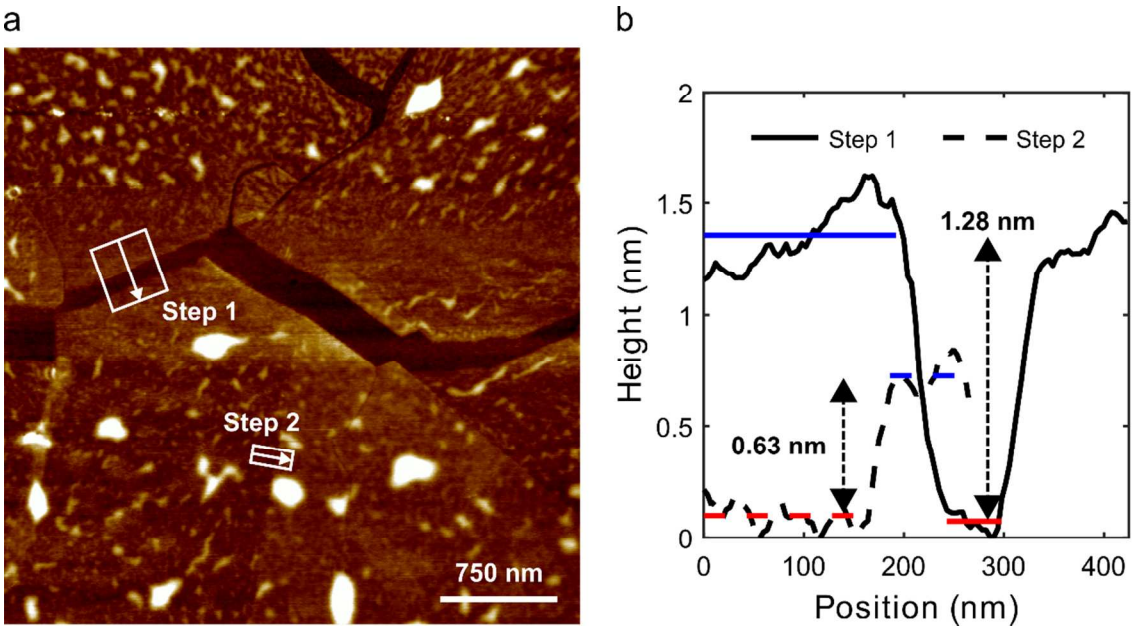

Figure S4. A tapping mode AFM image taken of the MoS_2 on Al_2O_3 sample a few months after the PFM measurement taken in Figure 5 is shown in (**a**). (**b**) shows step height profiles for the two boxes highlighted in (**a**). Step 1 shows a step from monolayer MoS_2, to the Al_2O_3 substrate, to another monolayer region. The AFM height is inflated from the expected monolayer thickness and is attributed to scanning over materials with different mechanical properties. Step 2 shows a monolayer to bilayer MoS_2 step with an expected thickness value.

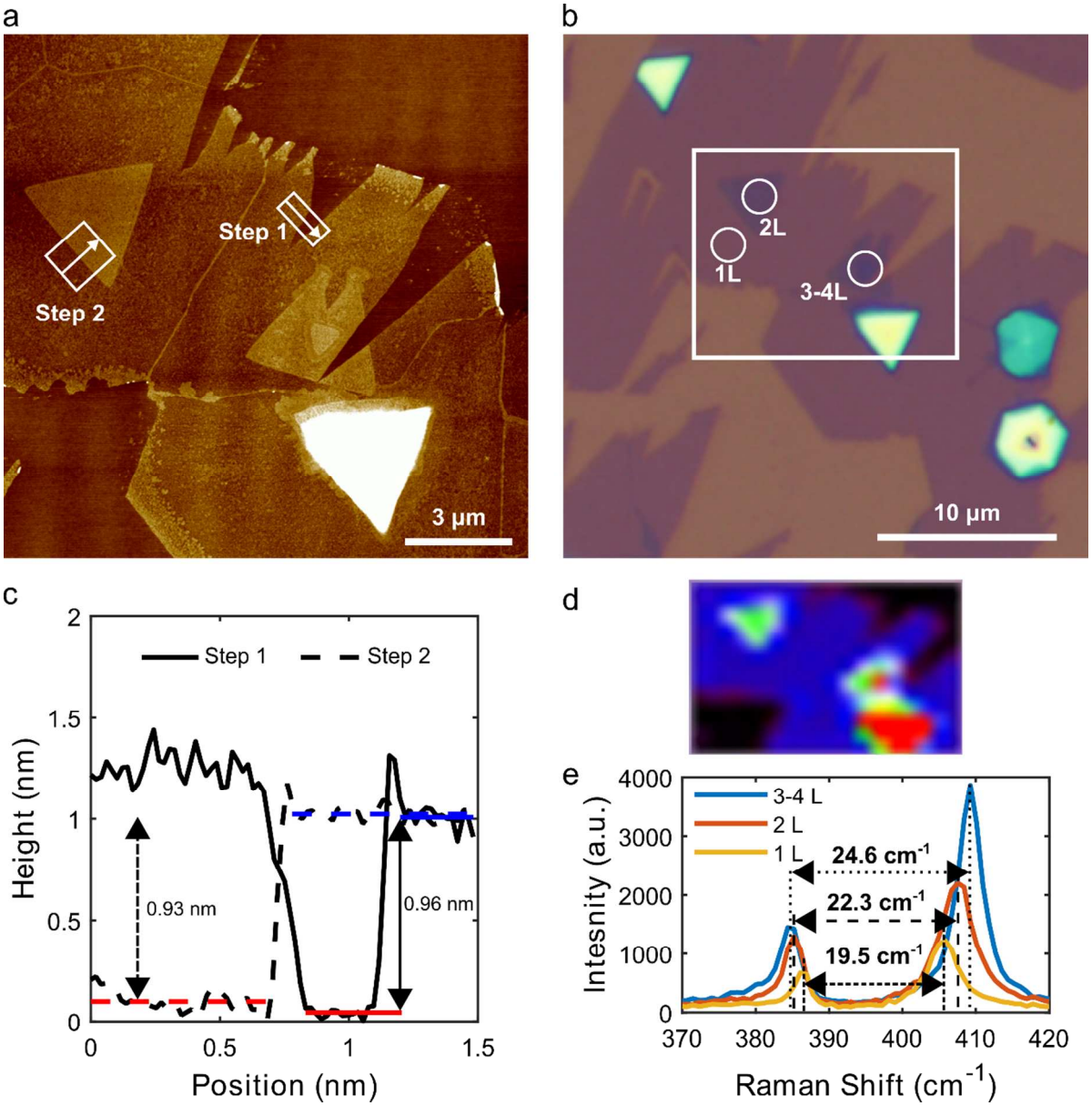

Figure S5. A tapping mode AFM image is shown in (**a**) with boxes representing areas in which step height measurements are taken and displayed in (**c**). An optical image is shown in (**b**), where the white box represents the area shown in (**d**) and depicts a color-coded Raman map. The color corresponds to the integrated intensity of the A_{1g} MoS_2 peak to the silicon peak at 520 cm^{-1}. As expected, the signal becomes stronger as thicker MoS_2 is measured. Raman spectra of the points circled in (**b**) are shown in (**e**). This confirms the presence of monolayer MoS_2.

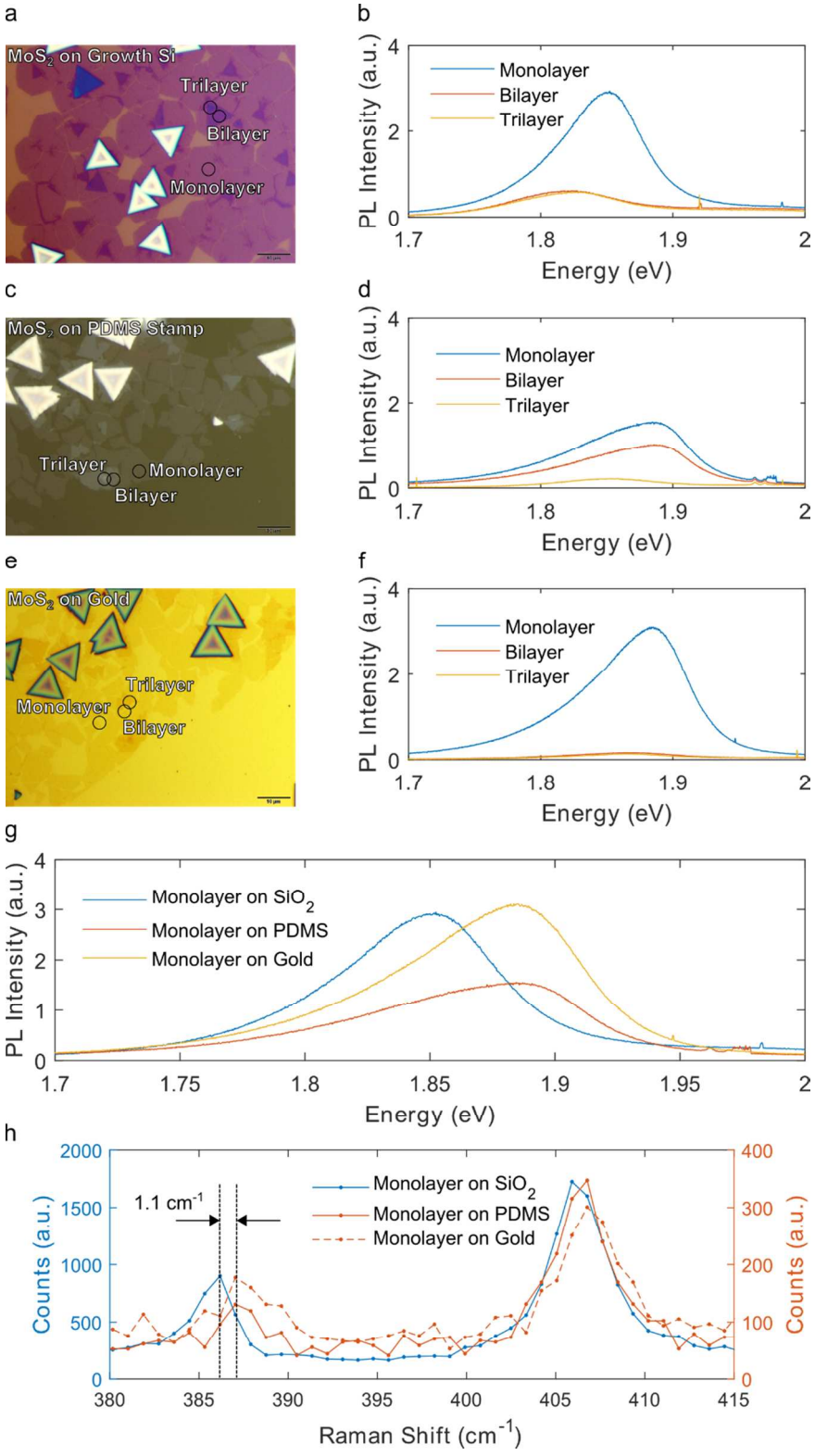

Figure S6. Microscope images of the MoS_2 on the growth substrate (**a**), PDMS stamp (**c**), and gold (**e**), with corresponding photoluminescence measurements (**b,d,f**). As expected, the monolayer MoS_2 has the

highest PL intensity because of its transition to a direct-gap semiconductor at the monolayer limit. PL and Raman data from the MoS_2 on the different substrates are shown together in (**g**) and (**h**), respectively, to show the peak shifts. The substrate can affect the peak locations on the PL signal[4], so PL alone is not reliable to determine strain. The E^1_{2g} Raman peak is sensitive to strain and can be used to estimate the amount of residual biaxial strain present in the MoS_2 while on the growth substrate of SiO_2[9]. With a shift of roughly 1.1 cm^{-1} in the E^1_{2g}, we estimate a residual tensile strain of 0.21 %.

Supporting Note 3: *Background Subtraction for d_{33}^{eff} Estimation*

Although **eq S1** is strictly correct, a background signal is always present regardless of the material that is being measured. To remove this background signal, which may be cantilever, sample, or PFM dependent, a background subtraction process is implemented which uses both the piezoresponse amplitude and piezoresponse phase channels.

First, a PFM image that includes monolayer MoS_2 and the exposed substrate is taken with the drive voltage (V_d) applied. Immediately following this, a second PFM image is taken without applying V_d to the sample. This allows for two different types of background measurements: one that measures the response of the substrate, and one that measures the error introduced by any tip motion during the scanning process or from the feedback electronics.

Second, values of the piezoresponse amplitude and piezoresponse phase for each material are gathered by averaging over areas that contain either monolayer MoS_2, exposed substrate, or any area for the V_{off} PFM image (there are no distinguishable differences in the piezoresponse amplitude or phase signal on the MoS_2 and substrate when V_d is not applied).

Vectors can now be constructed from the piezoresponse amplitude and piezoresponse phase measurements taken on the MoS_2, substrate, and V_{off} image. A background-subtracted piezoresponse amplitude estimate is then obtained by performing a vector subtraction of the background signal vector from the MoS_2 signal vector. The new piezoresponse amplitude of the background-subtracted vector is used in **eq S1** to estimate d_{33}^{eff}. This process is illustrated schematically in Figure 4.

The same subtraction procedure is applied with the MoS_2 and V_{off} vectors to obtain another estimate of d_{33}^{eff}. If there is little contribution to the signal measured on the MoS_2 by the substrate, the MoS_2-substrate and MoS_2-V_{off} d_{33}^{eff} estimates should be similar, which is indeed the case. Lastly, the contribution to the piezoresponse signal by the substrate can be estimated by doing a substrate-V_{off} vector subtraction. This yields order-of-magnitude smaller values than on the MoS_2, suggesting that the substrates used in this experiment are not responding electromechanically in the PFM measurements.

Supporting Note 4: *Uncertainty Estimation*

The uncertainty in the d_{33}^{eff} measurement is calculated by using error propagation of the measured values. To do this an equation must be created which incorporates all variables containing uncertainty. In this case, the equation for d_{33}^{eff} is

$$d_{33}^{eff} = \frac{S_d}{V_d \cdot g} \left|\overrightarrow{A^{BS}}\right|, \tag{S2}$$

where $\left|\overrightarrow{A^{BS}}\right|$ is the amplitude, in mV, of the background subtracted vector. $\left|\overrightarrow{A^{BS}}\right|$ can be expanded in terms of the measured values as

$$\left|\overrightarrow{A^{BS}}\right| = \sqrt{\left|\overrightarrow{A^{M}}\right|^2 + \left|\overrightarrow{A^{B}}\right|^2 - 2\left|\overrightarrow{A^{M}}\right|\left|\overrightarrow{A^{B}}\right|\cos(\theta^M - \theta^B)}\,, \tag{S3}$$

where $\left|\overrightarrow{A^{M}}\right|$, θ^M, $\left|\overrightarrow{A^{B}}\right|$, and θ^B are the amplitude and phase of the vector measured on the MoS_2 and background, respectively.

The uncertainty of $\left|\overrightarrow{A^{BS}}\right|$ can be obtained by using the formula

$$\sigma_{A-BS} = \sqrt{\left(\frac{\partial\left|\overrightarrow{A^{BS}}\right|}{\partial\left|\overrightarrow{A^{M}}\right|}\right)^2 \sigma_{AM}^2 + \left(\frac{\partial\left|\overrightarrow{A^{BS}}\right|}{\partial\left|\overrightarrow{A^{B}}\right|}\right)^2 \sigma_{AB}^2 + \left(\frac{\partial\left|\overrightarrow{A^{BS}}\right|}{\partial\theta^M}\right)^2 \sigma_{PM}^2 + \left(\frac{\partial\left|\overrightarrow{A^{BS}}\right|}{\partial\theta^B}\right)^2 \sigma_{PB}^2}\,, \tag{S4}$$

where σ_{AM}, σ_{AB}, σ_{PM}, σ_{PB}, are the uncertainties associated with the amplitude of the MoS_2 and background, and the phase of the MoS_2 and background, respectively. The values for the measured amplitudes and phases are obtained by performing a Gaussian fit over a distribution of points in the PFM measurement to find a mean value. The associated uncertainties are taken to be the 95% confidence interval of the fitted mean values. All calculations are done using MATLAB.

Next, the error must be propagated through **eq S2**. This can be done by using the equation

$$\sigma_d = d_{33}^{eff}\sqrt{\left(\frac{\sigma_s}{s_d}\right)^2 + \left(\frac{\sigma_V}{V_d}\right)^2 + \left(\frac{\sigma_{A-BS}}{\left|\vec{A^{BS}}\right|}\right)^2}, \tag{S5}$$

where σ_d, σ_s, and σ_V, are the uncertainties associated with d_{33}^{eff}, s_d, and V_d, respectively.

This value represents the uncertainty in the fitting of the mean value of the measurements. To incorporate any uncertainty originating from the substrate on the measurement, the d_{33}^{eff} calculated when comparing the substrate to the V_{off} condition can be thought of an error estimate. The total uncertainty can then be calculated as

$$\sigma_{tot} = \sqrt{{\sigma_d}^2 + {d_{33,sub-Voff}^{eff}}^2}. \tag{S6}$$

In **Table 1**, the calculated d_{33}^{eff} and σ_{tot} are shown for background subtraction of MoS_2 versus the substrate, MoS_2 versus the V_{off} condition, and d_{33}^{eff} and σ_d for comparing the substrate versus the V_{off} condition.

Supporting Note 5: *Voltage drop through MoS_2 on Al_2O_3*

Assuming that the electric flux density through the two materials is equal, we have

$$\epsilon_{MoS_2} E_{MoS_2} = \epsilon_{Al_2O_3} E_{Al_2O_3}. \tag{S7}$$

The electric field is given by

$$E_i = -\frac{V_i}{t_i} \tag{S8}$$

where t is the thickness of the material. Combining **eq S7** and **eq S8**, we obtain

$$\epsilon_{MoS_2} \frac{V_{MoS_2}}{t_{MoS_2}} = \epsilon_{Al_2O_3} \frac{V_{Al_2O_3}}{t_{Al_2O_3}}. \tag{S9}$$

Now, by using

$$V_{MoS_2} + V_{Al_2O_3} = V_d, \tag{S10}$$

where V_d is the drive voltage, we can obtain

$$V_{MoS_2} = V_d \frac{\epsilon_{Al_2O_3}/t_{Al_2O_3}}{\epsilon_{MoS_2}/t_{MoS_2} + \epsilon_{Al_2O_3}/t_{Al_2O_3}}. \tag{S11}$$

Supporting Note 6: *Determination of Drive Frequency for PFM*

The piezoresponse amplitude of the PFM measurement is in general frequency dependent. A typical frequency sweep of the piezoresponse amplitude on the MoS_2/gold sample is shown in Figure S7. This frequency dependence should not be of electromechanical origin, but instead is most likely caused by the measurement electronics. Similar frequency dependencies are seen with different cantilevers, different substrates, and when the drive voltage is not routed to the sample. This is another reason for doing a PFM measurement without applying the drive voltage to obtain a background signal.

The drive frequency used in the measurements must be away from the extraneous peaks in the piezoresponse amplitude frequency sweep as well as away from the clamped mechanical resonance point of the cantilever (roughly 800 kHz). The frequency 60 kHz is chosen because it is within a frequency independent region in the frequency sweep.

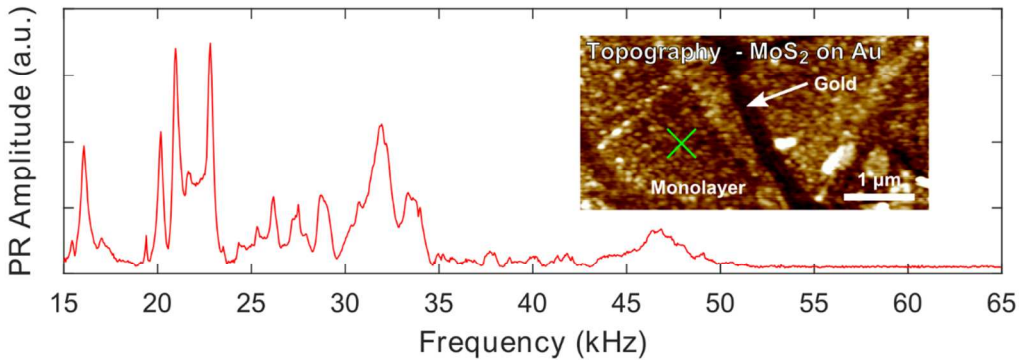

Figure S7. The PR amplitude vs drive voltage frequency measured on the MoS_2 on gold sample. The location of the measurement is denoted by the 'x' in the inset AFM topographic image. A chaotic relationship is seen at the lower frequencies, but at higher frequencies the PR amplitude becomes independent of frequency. 60 kHz is used in all PFM measurements to be well within the frequency independent region. These frequencies are well below the contact resonant point of the AFM cantilever.

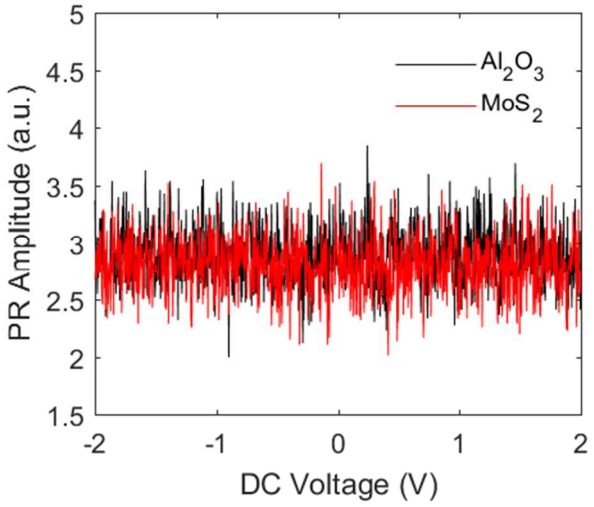

Figure S8. The PR amplitude measured as the DC voltage between the AFM tip and n^{++} Si is swept on the MoS_2 / Al_2O_3 sample. Measurements on both the MoS_2 and the Al_2O_3 show that the PR amplitude is independent from the DC voltage. This indicates that the electrostatic interactions and work-function differences are not significant.

Supporting Note 7: *Estimating* μ_{eff}^{*}

To estimate μ_{eff}^{*}, let us first better understand **eq 7** and **eq S1**. By doing a PFM measurement, converse piezoelectricity is used to effectively measure the strain caused by an applied electric field. Using the definition of strain,

$$\varepsilon_3 = \frac{\Delta z}{t}, \tag{S12}$$

where *Δz* is the vertical deflection measured by the PFM (piezoresponse amplitude) and *t* is the thickness of the material being measured, **eq 7** can be written as

$$d_{33}^{eff} = \frac{\Delta z}{tE_3}. \tag{S13}$$

This is similar to **eq S1** where *Δz* contains the deflection sensitivity and the gain factor, and therefore represents the actual deflection of the sample.

Now consider the different components in **eq 9** which may be present in MoS_2 if we assume that the electric field is perpendicular to the surface of the gold and MoS_2:

$$\sigma_1 = \mu_{19}^{*} \frac{\partial E_3}{\partial x_3}, \tag{S14a}$$

$$\sigma_2 = \mu_{19}^{*} \frac{\partial E_3}{\partial x_3}, \tag{S14b}$$

$$\sigma_3 = \mu_{39}^{*} \frac{\partial E_3}{\partial x_3}, \tag{S14c}$$

$$\sigma_4 = \mu_{48}^{*} \frac{\partial E_3}{\partial x_2}, \tag{S14d}$$

$$\sigma_5 = \mu_{48}^{*} \frac{\partial E_3}{\partial x_1}. \tag{S14e}$$

Of these components, σ_1 and σ_2 will create in-plane stress which may or may not create out-of-plane displacement due to Poisson-like effects. In **eq S14d** and **eq S14e**, the out-of-plane shear stress contributions σ_4 and σ_5 could create contributes to measured out-of-plane displacement. The most likely out-of-plane displacement would be due to **eq S14c** where an out-of-plane electric field changing in the z-

direction causes stress is the z-direction. This is plausible because the gradient is taken over the very short distance of a single monolayer of MoS_2.

For simplicity, we assume that the geometry and response of the system is approximated by **eq S14c** and substitute μ^*_{eff} for μ^*_{39}. Next, we assume that the dominant electric field derivative term, $\partial E_3/\partial x_3$, can be approximated, at these small length scales, as $\partial E_3/\partial x_3 \approx 2V_d/t^2$. This assumption corresponds to a linear dependence of E_3 on x_3, and a quadratic dependence of the electrostatic potential on x_3, within the MoS_2 layer, subject to the boundary conditions that E_3 vanish in the metal tip and sample contact, and that the total potential drop across the MoS_2 layer be V_d. Finally, using $\sigma = Y\varepsilon$ and **eq S13**, **eq 9** can be rewritten as

$$\mu^*_{eff} = \frac{\Delta z}{V_d} \cdot Y \cdot \frac{t}{2} = d^{eff}_{33} \cdot Y \cdot \frac{t}{2}. \quad \text{(S17)}$$

Assuming Y = 270 GPa and t = 0.65 nm for monolayer MoS_2, **eq S17** yields 0.08 nC/m and 0.12 nC/m, based on PFM measurements for MoS_2 on gold and Al_2O_3/Si, respectively. This serves only as an order-of-magnitude estimate of μ^*_{eff}.

Supporting Note 8: *Electromechanical Response with Increasing MoS_2 Thickness*

Detailed analysis of the effect of thickness on the calculations is beyond the scope of this paper, but should be addressed briefly. Piezoelectricity does depend on the number of layers present as shown in literature[10,11]. Few-, odd-number layers of MoS_2 have a symmetry such that no inversion symmetry point is present, resulting in in-plane piezoelectricity. Even-layered MoS_2, on the other hand, has a different symmetry which has an inversion symmetry point and is thus not piezoelectric. Additionally, as the number of odd-layers increases to 3, 5, 7, etc., the in-plane MoS_2 can increasingly be considered 'bulk' which is not piezoelectric. The result is a stark decrease in the piezoelectric response as the number of layers increase, as is confirmed in references[10,11]. It should be emphasized that regardless of the number of layers present, these piezoelectric responses are only within the plane of the MoS_2 film.

Flexoelectricity is more difficult to analyze with increasing thickness. As MoS_2 transitions from odd-number to even-number layer, its point group changes from D_{3h} to D_{3d}, respectively. The resulting flexoelectric tensors are different from each other[12], but still have non-zero out-of-plane coefficients, namely μ^*_{39}. These differences make it more difficult to directly compare even- and odd-numbered layers of MoS_2 by using the PFM technique, especially since we are grouping the total response into the effective value μ^*_{eff}. Moreover, our estimates for μ^*_{eff} rely on estimates of the electric field distribution throughout the thickness of MoS_2. This field distribution will certainly change with increasing layer thickness and is beyond the scope of this paper to calculate. These issues are a subject of ongoing investigation and may be the subject of a future publication.

Supporting Note 9: *XPS Measurements*

XPS measurements were performed to look for surface contaminants that could affect the PFM signal. Three separate samples were measured: 1) the MoS_2 on gold sample for which PFM images are shown in Figure 3**,** 2) gold deposited on an Si/SiO_2 substrate, 3) gold deposited on an Si/SiO_2 substrate that was stamped by PDMS without MoS_2. **Supporting Table S1** shows the concentration of various elements detected on the surfaces of the samples.

A notable amount of carbon is detected on all of the samples, most of which is probably from adventitious carbon which is found on all samples exposed to air. The samples which were stamped with PDMS show increased levels of oxygen and silicon compared to the non-stamped gold sample. Residue left on the sample from the stamping process, or unreacted MoO_3 from the CVD growth processes most-likely is the culprit of the increase. Since the silicon and oxygen increase is also seen on the gold sample without the MoS_2, it is assumed that any PDMS residue is blanket-deposited wherever the PDMS contacts and does not preferably attach to the MoS_2. This means that if the PDMS residue contributes to the PFM signal, its contribution to the MoS_2 signal can be removed by doing the background subtraction process of the substrate/residue PFM measurement. One possible complication would be if the PDMS residue

interacts differently with the MoS_2 versus the gold or Al_2O_3 substrates. More work is needed to rule out any such effects.

We also note that the typical magnetic lens used for XPS measurements could not be used for the MoS_2/gold sample because it was mounted on a magnetic AFM disk for better electrical contact during PFM measurements. Only the electrostatic lens was used for this sample, so the % concentration values may not be precise and represent a broader range of possible percentages.

Table S1. Percent concentration of selected elements on the surface of three different samples using XPS.

Element	Gold Only	PDMS-Stamped Gold	MoS_2 on Gold
Au	62.0 %	56.4 %	37.3 %
C	34.2 %	35.2 %	39.0 %
O	3.8 %	6.0 %	16.1 %
Si	0 %	2.4 %	5.6 %
Mo	0 %	0 %	0.9 %
S	0 %	0 %	1.1 %

References

(1) Shearer, C. J.; Slattery, A. D.; Stapleton, A. J.; Shapter, J. G.; Gibson, C. T. *Nanotechnology 27*, 0.

(2) Nemes-Incze, P.; Osváth, Z.; Kamarás, K.; Biró, L. P. *Carbon N. Y.* **2008**, *46*, 1435–1442.

(3) Castellanos-Gomez, A.; Roldán, R.; Cappelluti, E.; Buscema, M.; Guinea, F.; van der Zant, H. S. J.; Steele, G. a. *Nano Lett.* **2013**, *13*, 5361–5366.

(4) Buscema, M.; Steele, G. A.; van der Zant, H. S. J.; Castellanos-Gomez, A. *Nano Res.* **2014**, *7*, 561–571.

(5) Brennan, C. J.; Nguyen, J.; Yu, E. T.; Lu, N. *Adv. Mater. Interfaces* **2015**, *2*, 1500176.

(6) Man, M. K. L.; Deckoff-Jones, S.; Winchester, A.; Shi, G.; Gupta, G.; Mohite, A. D.; Kar, S.; Kioupakis, E.; Talapatra, S.; Dani, K. M. *Sci. Rep.* **2016**, *6*, 20890.

(7) Bhattacharjee, S.; Ganapathi, K. L.; Chandrasekar, H.; Paul, T.; Mohan, S.; Ghosh, A.; Raghavan, S.; Bhat, N. *Adv. Electron. Mater.* **2017**, *3*, 1–9.

(8) Dumcenco, D.; Ovchinnikov, D.; Marinov, K.; Lazić, P.; Gibertini, M.; Marzari, N.; Sanchez, O. L.; Kung, Y.-C.; Krasnozhon, D.; Chen, M.-W.; Bertolazzi, S.; Gillet, P.; Fontcuberta i Morral, A.; Radenovic, A.; Kis, A. *ACS Nano* **2015**, *9*, 4611–4620.

(9) Lloyd, D.; Liu, X.; Christopher, J. W.; Cantley, L.; Wadehra, A.; Kim, B. L.; Goldberg, B. B.; Swan, A. K.; Bunch, J. S. *Nano Lett.* **2016**, *16*, 5836–5841.

(10) Wu, W.; Wang, L.; Li, Y.; Zhang, F.; Lin, L.; Niu, S.; Chenet, D.; Zhang, X.; Hao, Y.; Heinz, T. F.; Hone, J.; Wang, Z. L. *Nature* **2014**, *514*, 470–474.

(11) Zhu, H.; Wang, Y.; Xiao, J.; Liu, M.; Xiong, S.; Wong, Z. J.; Ye, Z.; Ye, Y.; Yin, X.; Zhang, X. *Nat. Nanotechnol.* **2014**, *10*, 151–155.

(12) Shu, L.; Wei, X.; Pang, T.; Yao, X.; Wang, C. *J. Appl. Phys.* **2011**, *110*, 104106.